Novel small molecule FGF23 inhibitors increase serum phosphate and improve skeletal abnormalities in *Hyp* mice

Zhousheng Xiao, Jiawang Liu, Shih-Hsien Liu, Loukas Petridis, Chun Cai, Li Cao, Guangwei Wang, Ai Lin Chin, Jacob W. Cleveland, Munachi O. Ikedionwu, Jesse D. Carrick, Jeremy C. Smith, Leigh Darryl Quarles

Molecular Pharmacology; MOLPHARM-AR-2021-000471

Figure S1

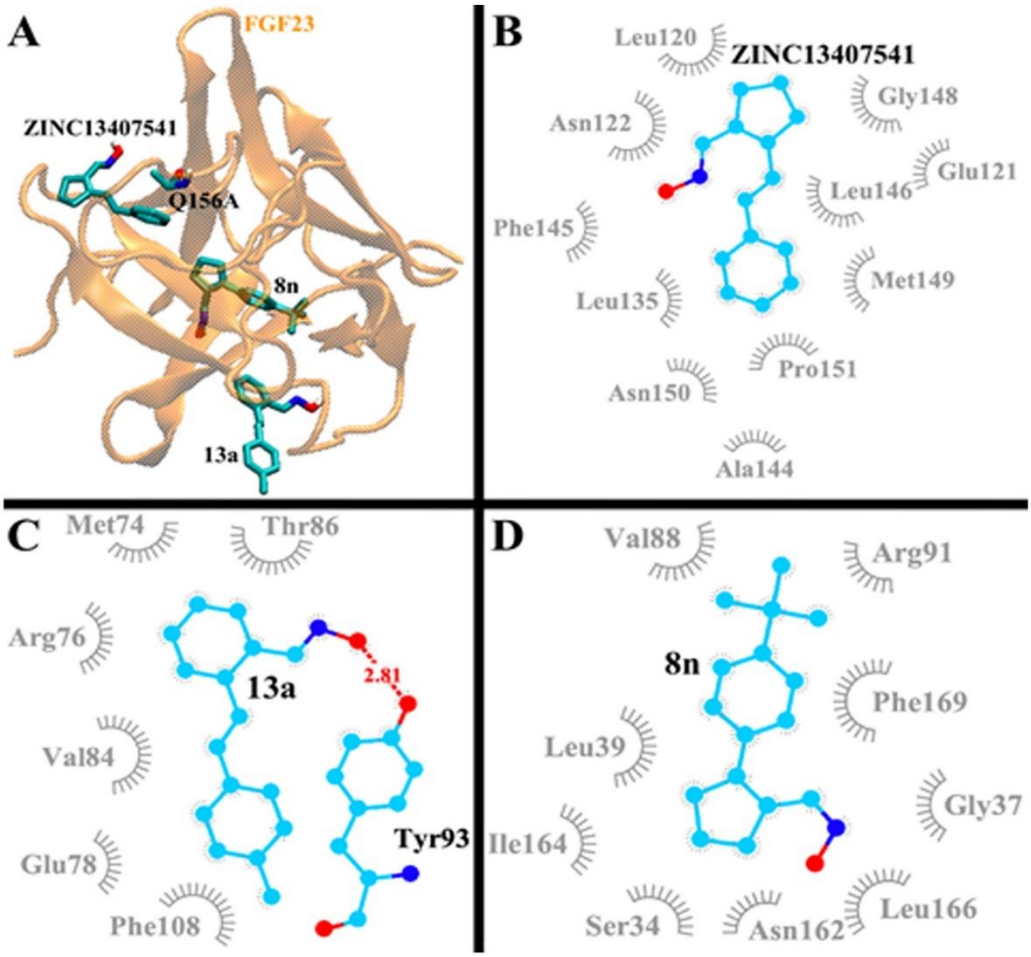

Figure S1. The computationally predicted interaction of ZINC13407541 and its two analogs, **13a** and **8n**, with the N-terminal domain of FGF23 (PDB code: 5W21) Q156A mutant shown in (A) 3D structure; in (B) (C) and (D) 2D residue-contacting map for ZINC13407541, **13a**, and **8n**, respectively. Hydrogen bonds are shown in red dash lines with donor-acceptor distances in Å. Hydrophobic interactions are shown in gray. The corresponding estimated free energies of binding (ΔG) for the three poses are shown in Table S5.

Table S1. The raw results of hydrogen-bond analyses on binding poses of ZINC13407541 to the N-terminal domain of FGF23 in the molecular docking. The residue in bold forms two hydrogen bonds with the ligand. Otherwise, one hydrogen bond is formed.

Pose	ΔG [kcal/mol]	Residue 1	Residue 2	Residue 3	Residue 4
1	-7.0	Asn122	Gln156		
2	-6.9	Asn122	Gln156		
3	-6.6	Arg76	Ser77		
4	-6.4	Met74	Arg76	Val84	Thr86
5	-6.4				
6	-6.2	Tyr93			
7	-6.1	Tyr93			
8	-6.0	Arg76	Ser77		
9	-5.8	Thr86			
10	-5.7	Leu146			
11	-5.6	Tyr93			
12	-5.2	Gly38	**Ile75**		
13	-5.0	Glu78			
14	-5.0				
15	-5.0	Ser159			
16	-5.0	Gln156			
17	-4.9	Thr119			
18	-4.9	Gln118			
19	-4.9				
20	-4.8				

Table S2. The raw results of hydrogen-bond analyses on binding poses of 13a to the N-terminal domain of FGF23 in the molecular docking. The residue in bold forms two hydrogen bonds with the ligand. Otherwise, one hydrogen bond is formed.

Pose	ΔG [kcal/mol]	Residue 1	Residue 2	Residue 3	Residue 4
1	-7.3	Asn122	Gln156		
2	-6.9				
3	-6.9	Tyr93			
4	-6.8	Tyr93			
5	-6.7	Met74	Arg76	Val84	Thr86
6	-6.7	Tyr93			
7	-6.6	Ser77			
8	-6.2	Ala45	Gln156		
9	-6.2	Arg76	Ser77		
10	-6.1	Thr86			
11	-5.9				
12	-5.9	Leu146			
13	-5.9	Gln156			
14	-5.7	Tyr93			
15	-5.7	Pro152	Ser155	Gln156	
16	-5.7				
17	-5.7	**Gln67**			
18	-5.7	Asn49	Tyr154		
19	-5.6	Thr86			
20	-5.5				

Table S3. The raw results of hydrogen-bond analyses on binding poses of 8n to the N-terminal domain of FGF23 in the molecular docking. The residues in bold each form two hydrogen bonds with the ligand. Otherwise, one hydrogen bond is formed.

Pose	ΔG [kcal/mol]	Residue 1	Residue 2	Residue 3	Residue 4
1	-6.5				
2	-5.9	Ser137	Gly139		
3	-5.8	Gln156			
4	-5.8	Thr46	Asn49	Tyr154	
5	-5.8	Tyr93			
6	-5.8	Tyr93			
7	-5.8	Thr86			
8	-5.8	Ser77			
9	-5.6	Leu146			
10	-5.4				
11	-5.4	Tyr93			
12	-5.4	Met74	Arg76	Val84	Thr86
13	-5.4				
14	-5.3				
15	-5.3	Arg76			
16	-5.3	Tyr154	Ser155	**Gln156**	
17	-5.2	Ser34	Asn162	Ile164	
18	-5.2	Gly38	**Ile75**		
19	-5.2	Pro152	Ser155	Gln156	
20	-5.1	Asp125	Tyr127	Ser159	

Table S4. The conservation scores in descending order of the residues shown in Table 1 in the main text. These scores were estimated by The ConSurf Server with 1 being the least conserved and 9 being the most conserved.

Residue	Conservation score
Gln67	9
Asp125	9
Ser137	9
Pro152	9
Asn162	9
Asn122	8
Tyr127	8
Ser155	8
Gln156	8
Ala45	7
Ile75	7
Glu78	7
Gly139	7
Ser159	7
Ser34	6
Val84	6
Ile164	6
Thr46	5
Arg76	5
Ser77	5
Asn49	4
Thr119	4
Gly38	3
Tyr93	3
Tyr154	3
Met74	2
Thr86	2
Gln118	1
Leu146	1

Table S5. The computationally estimated free energies of binding (ΔG) with standard errors of ZINC13407541, **13a**, and **8n** to the N-terminal domain of FGF23 Q156A mutant using AutoDock VinaMPI and K_{DEEP}. The corresponding binding poses of ligands are shown in **Fig. S1**.

Compound	**ΔG(VinaMPI) [kcal/mol]**	**ΔG(K_{DEEP}) [kcal/mol]**
ZINC13407541	-6.5 ± 2.9	-5.6 ± 0.7
13a	-6.9 ± 2.9	-7.0 ± 0.5
8n	-6.4 ± 2.9	-6.0 ± 0.5

The PDB captions

FGF23.pdb
PDB_5W21.pdb

ZINC13407541/
ZINC13407541/ZINC13407541_Pose_1.pdb
ZINC13407541/ZINC13407541_Pose_2.pdb
ZINC13407541/ZINC13407541_Pose_3.pdb
ZINC13407541/ZINC13407541_Pose_4.pdb
ZINC13407541/ZINC13407541_Pose_5.pdb
ZINC13407541/ZINC13407541_Pose_6.pdb
ZINC13407541/ZINC13407541_Pose_7.pdb
ZINC13407541/ZINC13407541_Pose_8.pdb
ZINC13407541/ZINC13407541_Pose_9.pdb
ZINC13407541/ZINC13407541_Pose_10.pdb
ZINC13407541/ZINC13407541_Pose_11.pdb
ZINC13407541/ZINC13407541_Pose_12.pdb
ZINC13407541/ZINC13407541_Pose_13.pdb
ZINC13407541/ZINC13407541_Pose_14.pdb
ZINC13407541/ZINC13407541_Pose_15.pdb
ZINC13407541/ZINC13407541_Pose_16.pdb
ZINC13407541/ZINC13407541_Pose_17.pdb
ZINC13407541/ZINC13407541_Pose_18.pdb
ZINC13407541/ZINC13407541_Pose_19.pdb
ZINC13407541/ZINC13407541_Pose_20.pdb

13a/
13a/13a_Pose_1.pdb
13a/13a_Pose_2.pdb
13a/13a_Pose_3.pdb
13a/13a_Pose_4.pdb
13a/13a_Pose_5.pdb
13a/13a_Pose_6.pdb
13a/13a_Pose_7.pdb
13a/13a_Pose_8.pdb
13a/13a_Pose_9.pdb
13a/13a_Pose_10.pdb
13a/13a_Pose_11.pdb
13a/13a_Pose_12.pdb
13a/13a_Pose_13.pdb
13a/13a_Pose_14.pdb
13a/13a_Pose_15.pdb
13a/13a_Pose_16.pdb
13a/13a_Pose_17.pdb
13a/13a_Pose_18.pdb
13a/13a_Pose_19.pdb
13a/13a_Pose_20.pdb

8n/
8n/8n_Pose_1.pdb

8n/8n_Pose_2.pdb
8n/8n_Pose_3.pdb
8n/8n_Pose_4.pdb
8n/8n_Pose_5.pdb
8n/8n_Pose_6.pdb
8n/8n_Pose_7.pdb
8n/8n_Pose_8.pdb
8n/8n_Pose_9.pdb
8n/8n_Pose_10.pdb
8n/8n_Pose_11.pdb
8n/8n_Pose_12.pdb
8n/8n_Pose_13.pdb
8n/8n_Pose_14.pdb
8n/8n_Pose_15.pdb
8n/8n_Pose_16.pdb
8n/8n_Pose_17.pdb
8n/8n_Pose_18.pdb
8n/8n_Pose_19.pdb
8n/8n_Pose_20.pdb

Q156A/
Q156A/FGF23_Q156A.pdb
Q156A/ZINC13407541_Pose_1.pdb
Q156A/13a_Pose_1.pdb
Q156A/8n_Pose_1.pdb